Generation of High-Resolution Mosaic for Photo-Realistic Texture-Mapping of Cultural Heritage 3D Models

Fabio Remondino and Jana Niederoest
Institute for Geodesy and Photogrammetry
ETH Zurich, Switzerland
E-mail: <fabio><jana>@geod.baug.ethz.ch
Web: http://www.photogrammetry.ethz.ch

Abstract

The work investigates the problem of how information contained in different overlapping images of a scene can be combined to produce larger images of higher quality. The resulted images can be used for different applications like forensic image analysis, computer animation, special effects, 3D model texture mapping or panorama mosaic. In our case, high-resolution image mosaics of mural frescos are required for the texturing of a 3D model that will be used in a movie production. We developed a novel method for the derivation of a high quality mosaic using multi-resolution and multi-temporal images acquired from arbitrary positions and cameras. This method named 'constrained mesh-wise affine transformation' allows for seamless enhancement of the scene in the areas where higher resolution images are available. In this paper, we also discuss alternative procedures for the texture mapping of a 3D model using existing multi-resolution and multi-temporal imagery. The work has been done within a project aimed at a virtual and physical reconstruction of the destroyed Buddha statues of Bamiyan, Afghanistan.

1. Introduction

The generation of image mosaic has been deeply investigated in the last years. A mosaic is an image constructed by sticking together many other images, with the main goal of enlarging the field of view ('panorama') but also of increasing the spatial resolution, reducing the noise and eliminating moving objects or blur. Image mosaicing involves the geometric registration and radiometric correction of different images, possibly acquired from the same position. In the vision community, the mosaicing with the aim of restoring the poor quality of the input images, i.e. the generation of a higher-resolution image from lower resolution images, is called *super-resolution*. In the generated higher resolution image, the sharpness is improved and the pixel size is smaller than the lower resolution images. Usually a combination of deblurring and fine resolving is applied together with a transformation described in a simple parametric form or scene dependent. Various algorithms have been proposed for super-resolution [IP91, MP94, EF97, CB97, BS98, CZ98, BK00] and several software systems are available on the market [VI, VF]. Many algorithms work in the Fourier domain and are based on translational image motion, affine, biquadratic or planar projective image transformations. The success of the algorithms depends on the accuracy of the image processing model and a wrong transformation can degrade the final image rather than enhance it.

The generation of mosaic and higher resolution images has many possible applications, like forensic analysis, panorama mosaic or 3D model texture mapping. Concerning panoramic/mosaic images, more than 30 commercial systems are available on the market to mosaic images acquired with a rotating camera. The software distinguishes in the extent of the automation and in the requirements for the input data and, after the stitching, the panorama image is warped applying a particular projection for better visualization [PA].

In this article we report about several photogrammetric procedures to generate frescos image mosaics usable for the photo-realistic texturing of 3D digital models of cultural heritage scenes. The cultural heritage area is the Bamiyan valley, Afghanistan, while the frescos were located in the niche of the Great Buddha. The emphasis of the work is put on the use of various images of a non planar surface, acquired with different cameras, in different positions and at different time. Under these conditions, probably most of the common approaches and software systems would fail. We present a new method based on constrained mesh-wise affine transformation, which shows its capabilities for correct image mosaicing, edges straightness preservation and image sharpness (Section 4.3).

At first, the scope of the project and the frescos in the niche of a destroyed Great Buddha statue are described (Section 2), followed by the presentation of the available images for the required high-resolution mosaicing (Section 3). Then, we focus on the derivation of image mosaics using several methods such as planar projective image registration (Section 4.1), transformation between images and digital surface model (Section 4.2) and finally the mentioned constrained mesh-wise affine transformation, which delivered satisfactory results (Section 4.3). The full high-resolution mosaic is then used for the texture mapping of a 3D model. We describe this procedure in the Section 5 while also

discussing some alternative solutions for this purpose. The photogrammetrically reconstructed photo-realistic 3D model of the Buddha statue [GRZ04] including the texture-mapped niche will be used in a movie production which is planned to be shown in movie theatres and on TV in 2005.

2.   The Frescos in the Niches of Bamiyan

The famous Bamiyan Buddha statues, as well as other small statues in Foladi and Kakrak areas, have been destroyed by the Taleban militia in March 2001. In 2003 the World Heritage Committee has decided to include the cultural landscape and archaeological remains of the Bamiyan valley in the UNESCO World Heritage List [UN]. The whole area contains more than 750 caves and it is in a fragile state of conservation as it has suffered from abandonment, military actions and explosions. The major dangers are the risk of imminent collapse of the Buddha niches with the remaining fragments of the statues, further deterioration of still existing mural paintings in the caves, looting and illicit excavation. Among the destroyed Buddhas statues, the best known was the west Great Buddha. Its niche was excavated from the yellow rock of the cliff and is approximately 58 m high and 35 m depth at the base. The ceiling part of the niche (approximately 15 m of diameter and 16 m depth) was rich of mural paintings, of many different colours, representing Buddha-like figures, bright-coloured persons, ornaments, flowers and hanging curtains (Figure 1).
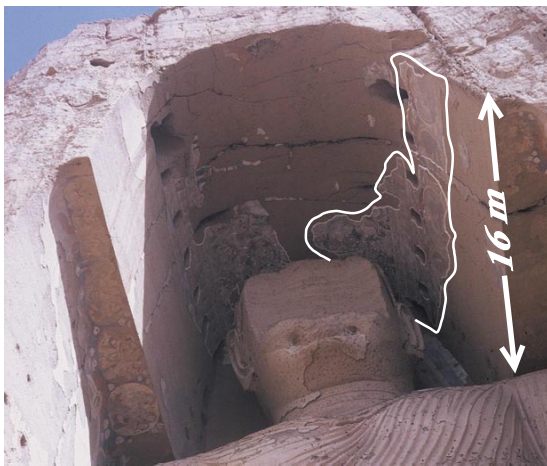

Figure 1: *The frescos in the ceiling of the Great Buddha niche. The marked area in the eastern part of the niche was the subject of the high-resolution mosaicing.*

In June 2003, a ceremony was held in front of the niche of the destroyed Great Buddha. The Minister of Information and Culture of the Transitional Islamic State of Afghanistan, the Ambassador of Japan and the Director of UNESCO's Afghanistan office, signed a joint protocol to assist in the preservation of the Buddhist mural paintings of the caves surrounding the large Buddha niches. As all the paintings of the two big niches have been destroyed during the explosions, the only way of documentation and visualization of the lost arts is the generation of an accurate and photo-realistic 3D model. For the digital reconstruction of the frescos a number of images taken before the destruction can be used.

3.   The Available Images

The available images of the eastern part of the Great Buddha niche were acquired with different cameras, from different positions and with different objectives. As the frescos are depicted on a cave ceiling, the images represent a non-planar surface and due to the different acquisition times their radiometry varies. Altogether 15 images depicting the eastern part of the frescos were available for mosaicing. Four of them show the full side of the ceiling in the low resolution; the rest eleven depict small details in high resolution (Figure 2, 3 and 4). All images - originally analogue diapositives - were scanned with a resolution of 20 microns.
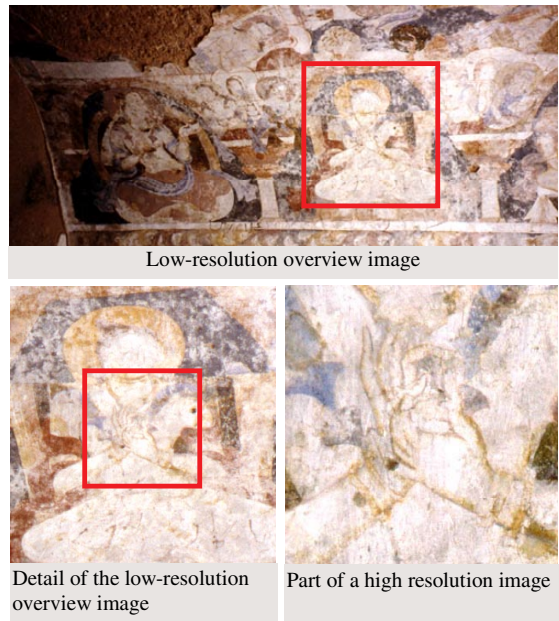

Low-resolution overview image

Detail of the low-resolution overview image

Part of a high resolution image

Figure 2: *One low-resolution overview image (above) and an enlarged detail of it (bottom left). The figure at bottom right depicts a central part of the left figure in another, high-resolution image.*
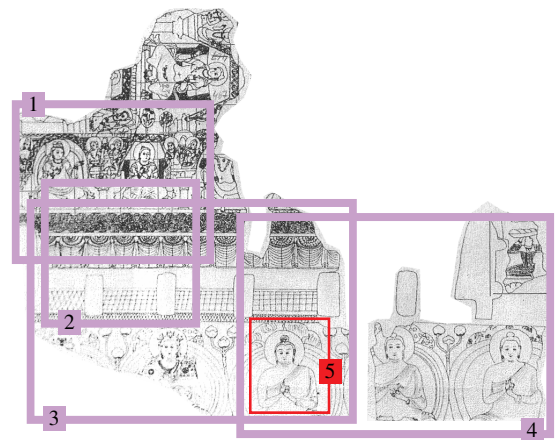

Figure 3: *Sketch of the whole fresco on the eastern side of the niche [BAM01] with the positions of 4 low- resolution images (No 1-4, thick lines) as well as one high-resolution image (No 5).*
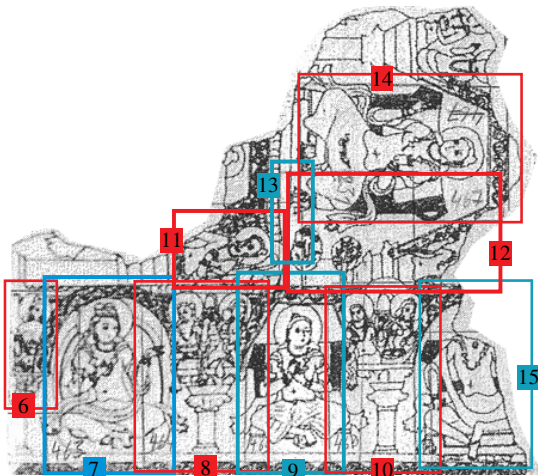
Figure 4: *Positions of 10 high-resolution images in the upper part of the fresco (No. 6-15).*

4. Generation of a High-Resolution Mosaic

In this section the procedures and results for the generation of a high-resolution mosaic are presented. We first describe a projective image registration, continue with the image rectification by using the Digital Surface Model (DSM) and end up with the description of the constrained mesh-wise transformation method.

4.1 Projective Image Registration

Two or more overlapping images can be considered related with a projective transformation (8 parameters) if:
1. The imaged scene is planar and there is an arbitrary camera motion (e.g. rotation and translation).
2. A generic 3D scene is imaged with a camera rotating around its vertical axis and/or zooming.
3. The camera is freely moving and viewing a very far away scene (e.g. aerial or satellite imagery).

In these cases, we can relate the 2D image correspondences to a unique 3D point. Feature based, direct or texture correlation based approaches [CZ98, IA00, SZE94] can be employed for the image registration and the parameters of the transformation are found using a maximum likelihood method or a least squares solution.

For the mosaicing of the 10 high-resolution images of the upper part of the fresco (Figure 4) we employed a commercial software package [PAN] as well as our own software for projective image transformation. Thank to rich texture details the definition of corresponding points between adjacent images was not a particular problem. As shown in Figure 5, the geometric registration is correctly performed and the radiometric adjustment could be easily done in image processing software (colour balance and brightness & contrast adjustment e.g. in Photoshop). However, the horizontal white edge is not preserved as straight as it must be (compare Figure 2 and Figure 5). In addition, the further combination of this projective mosaic with the other images was not possible, due to distorted geometry of the projective

mosaic. For these reasons we continued with the derivation of a full mosaic using alternative methods.

Figure 5: *A part of the mosaic generated with a projective transformation. Due to the non co-centric images and non planar scene, the straight edges such as the long horizontal line at the bottom are not preserved (dashed line in the upper image). The lower image shows the good geometric fit of three adjacent images in detail (arrows mark the beginning and the end of seamlines).*

4.2 Transformation between images and DSM

Having a Digital Surface Model (DSM) available, an image can be rectified using a projective transformation and at least 4 control points. The rectification can be performed if the DSM, in the area covered by the image, is planar or if the scene is far away from the camera. In our case, the most complicated part is to find control points between the highly detailed contents of the frescos, as now the frescos are gone. Therefore it would be possible to rectify and merge only image 3 and 4 of Figure 3, using the corners of the small windows as control information. Due to these problems, this kind of transformation could not be used for our case study.

4.3 Constrained Mesh-Wise Affine Transformation

The method called 'constrained mesh-wise affine transformation' allows for seamless combination of multi-resolution images of arbitrary geometry while preserving the original form of linear image features. The only pre-requisite is the existence of a suitable master image; into the geometry of this master image one or more (higher resolution) slave images will be transformed. As opposed to traditional affine or projective transformation, where the transformation parameters between two images are the same for the whole transformed image, the parameters of mesh-wise affine transformation have local validity. After defining a mesh of identical triangles in both images, the transformation parameters are determined for each corresponding triangle. Then, the image content of the slave image is transformed to the geometry of the master image triangle by triangle (Figure 6). Such mesh-wise approach has been used e.g. for the geometric correction of historical maps, where the old map is transformed to the geometry of a modern "master" map

[FSM98, Bal00, Nie02]. For the derivation of the high-resolution image mosaics we constrain the triangular mesh generation by defining some 'breaklines' along the linear image features, in order to avoid possible deformations after the transformation.
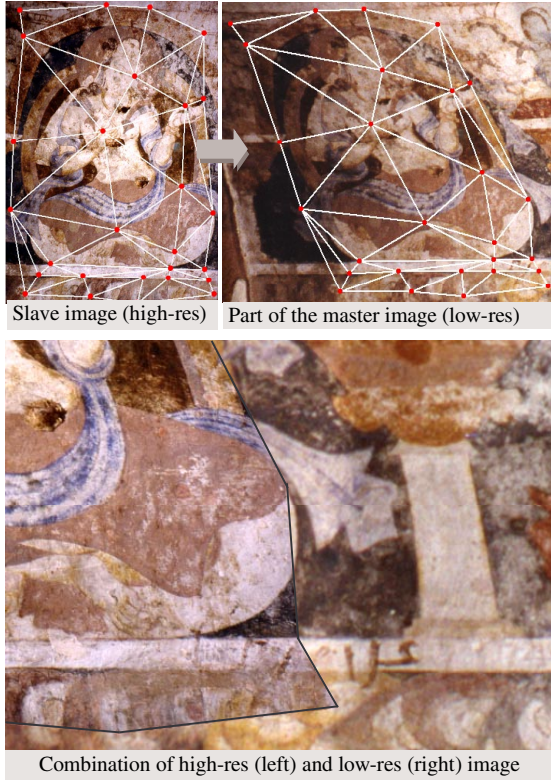

Slave image (high-res)   Part of the master image (low-res)

Combination of high-res (left) and low-res (right) image

Figure 6: *Principle of a constrained mesh-wise affine transformation (above) and a final upsampled master image (below, before radiometric adjustment).*

The algorithm works in the following way:

1. Definition of identical points between master and slave image. The measurement of the image coordinates can be performed manually or semi-automatically with least square matching.

2. Generation of the triangular mesh. It is important to define the triangles in the master image and then project them to the slave image (not vice versa). In this way the deformation of the defined triangles due to the different image geometries can be avoided. Moreover, in order to preserve linear image features, they must be assigned as 'breaklines' or constrains for the triangulation. For this purpose, identical points lying on the to-be-preserved line must be defined and connected along the line. If the definition of constrains is not done correctly (i.e. if the triangle edge cross the line without an identical point), the originally straight lines could break on that particular triangle edge after the transformation. A good transition between adjacent high-resolution images can be achieved by the use of same triangles at the image borders. The triangulation can be done either automatically (in case that the Delaunay triangulator can deal with the given constrains) or manually.

3. Computation of transformation parameters for each corresponding triangle. The planar affine 6-parameters transformation is applied for this purpose:

$$X_i = a_1 + a_2 \cdot x_i - a_3 \cdot y_i$$
$$Y_i = a_4 + a_5 \cdot x_i + a_6 \cdot y_i \tag{1}$$

with X_i, Y_i- coordinates in the master image
   x_i, y_i - coordinates in the slave image
   a_1-a_6 - unknown transformation parameters

As there are always 3 identical points and thus 6 observations, the searched 6 unknown parameters can be easily obtained without adjustment.

4. Transformation of the slave image triangle by triangle. For each pixel X_i, Y_i of the new transformed image, the algorithm finds a triangle in which it lies. This is done by defining a horizontal rightward line starting from the actual pixel and computing the number of its intersections with each triangle. When this number is one, the pixel must lay in that particular triangle. Using the 6 transformation parameters a_1-a_6 of this triangle, the corresponding pixel in the slave image is found by the inverse affine transformation:

$$x_i = \frac{a_3}{a_2} \cdot \frac{a_2 \cdot (Y_i - a_4) - a_5 \cdot (X_i - a_1)}{a_3 \cdot a_5 + a_2 \cdot a_6} + \frac{X_i - a_1}{a_2}$$
$$y_i = \frac{a_2 \cdot (Y_i - a_4) - a_5 \cdot (X_i - a_1)}{a_3 \cdot a_5 + a_2 \cdot a_6} \tag{2}$$

The grey value of the pixel at the position x_i, y_i is taken for colouring the actual pixel X_i, Y_i of the new transformed image.

When more slave images of different resolutions are transformed to the geometry of the master image, the result will be a multi-resolution image. Its number of pixels in both directions and the pixel size in object space (pixel footprint) are determined as follows:

1. Estimation of a pixel footprint for the master image as well as for all slave images. In our case, the pixel size in object space was approximately 15 mm for the master image and 3 mm for all slave images. For better co-referencing of the transformed images, we performed the computation in object space; thus, all the image coordinates are multiplied by the corresponding pixel footprint before the transformation.

2. Determination of a transformation scale for each slave image. As the parameters of mesh-wise affine transformation are only valid within each particular triangle, the transformation scale can be approximated as an average of scale parameters of all triangles. For our slave images we obtained average scale factors of 1.8-2.0.

3. Definition of a pixel size of each transformed slave image by multiplying the original pixel footprint with an approximated transformation scale. This value can be rounded up reasonably. We have set an object space pixel size of 5 mm for all transformed slave images. The reason for the increase of the pixel size is the fact that most of the

original slave images are frontal in respect to the photographed wall, whereas the master image (which is a "template" for all transformed images) was acquired from an oblique angle. Moreover, as the slave images depict only a small part of the scene, they represent nearly planar object, what is not the case by larger master image.

4. Final geometric mosaicing. The transformed slave images are composed and combined with the master image. The number of pixels and the geometric resolution of the final image are given by the transformed slave images, in general by a slave image with the highest resolution. The master image in the background is resized accordingly (Figure 7). In the described example it needed to be magnified 3-times (ratio between the original pixel footprint of 15 mm and final one of 5 mm). Thus, the master image has in fact the same resolution as the transformed slave images (5 mm), but its grey values are identical for groups of 3 x 3 pixels.
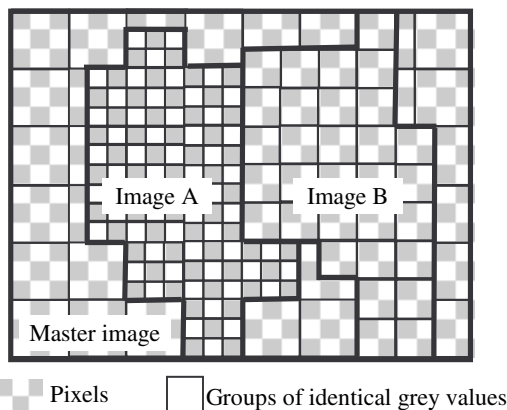

Figure 7: *Multi-resolution principle of the final mosaic obtained by the constrained mesh-wise transformation. The pixel size and number of pixels are given by the highest-resolution image (image A). The other images are resized accordingly; their grey values are not anymore unique for each pixel (image B and master image).*

Once all images are registered together, the radiometric differences between the adjacent images can be adjusted. We use commercial image processing packages for this purpose (colour balance and brightness & contrast adjustment in Photoshop). Figure 8 and Figure 9 show the result of mosaicing in the upper and bottom part of the fresco. The upper part is a composition of 12 images. Seven of them (No. 6-12 of Figure 4) were transformed to the geometry of the master image (No. 1 of Figure 3) using the mesh-wise approach. The other 4 border images (No. 2, 13, 14, 15 in Figure 3 and Figure 4) were transformed by applying the traditional affine or projective transformation as described in Section 4.1, because they were not completely depicted in the master image. The lower part of the fresco instead consists of 3 images (No. 3, 4 and 5 of Figure 3). Two of them were registered together with a projective transformation and then superimposed by the third, high-resolution image obtained by a mesh-wise affine transformation (Figure 9).
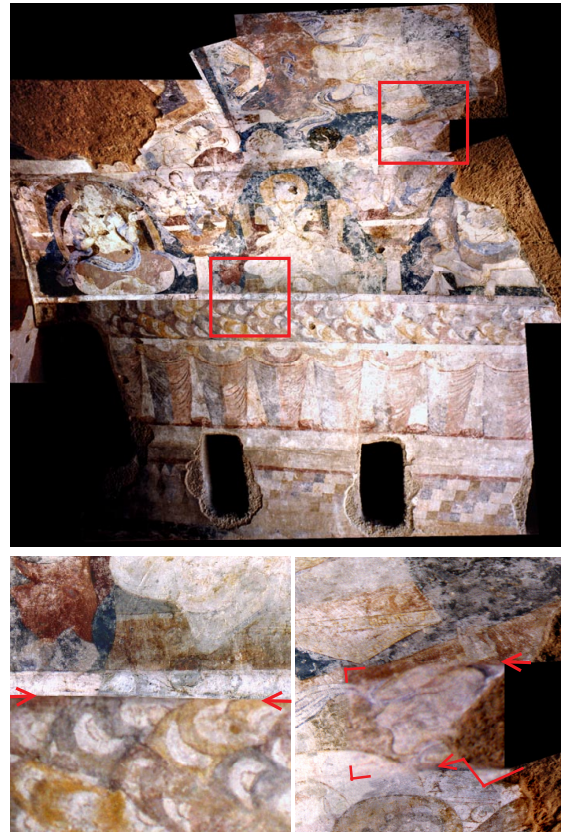

Figure 8: *Final high-resolution mosaic of the upper part of the fresco (composition of 12 images) and two detailed views of the high-resolution contents of the frescos (arrows and line segments mark the transition between adjacent low- and high-resolution images).*
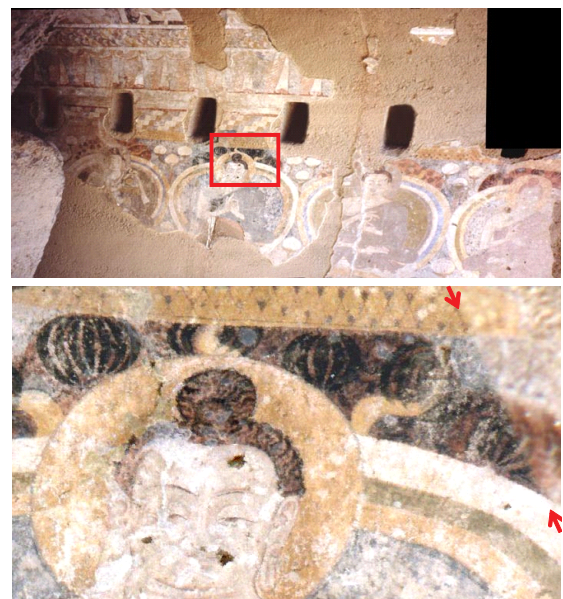

Figure 9: *Final high-resolution mosaic of the bottom part of the fresco (composition of 3 images, above). Below, a detail of a high-resolution image with a line (marked by the two arrows) to separate the low-resolution part is shown.*

5.   Texture Mapping

Once a 3D digital model of a scene is created, with the technique of texture mapping, grey-scale or true colour images are mapped onto the 3D geometric surface in order to achieve photo-realistic virtual models. Knowing the parameters of interior and exterior orientation of the cameras, to each triangular face of the 3D surface the corresponding image coordinates are calculated. Then the gray-scale or colour RGB values within the projected triangle are attached to the face. Usually texture mapping is performed using a frontal image for a related part of the object. Unfortunately in close-range applications this is often not satisfactory, due to varying light conditions during image acquisition and not enough image information for fully or partially occluded object parts. To overcome these problems, different pre-processing techniques and methods of texture mapping were developed [NB95, HLM96, DTM96, PAD98, VZG01, RCM02, BR03, KP04] based on weighted functions related to the camera's viewing angle or combinations of optimal image patches for each triangle of the 3D model or computing a 'ratio lighting' of the textures and derive a common light from them.

Often different factors affect the photo-realism of the textured 3D virtual model:

- Image radiometric distortion: this effect comes from the use of different images acquired in different positions or with different cameras or in different daily moments (e.g. varying light conditions). Therefore in the 3D textured model discontinuities and artifacts are present along the edges of adjacent triangles textured with different images. To avoid these, blending methods based on weighted functions can be used.

- Image dynamic range: digital images have always a lower dynamic range than the scene. Therefore bright areas are often saturated while dark parts contain low signal to noise (S/N) ratio. Radiometric adjustment can be performed with common image processing tools.

- Scene geometric distortion: this kind of error is generated from an incorrect camera calibration and orientation, an imprecise image registration, too large triangles mesh or errors in the surface reconstruction. All these sources do not preserve detailed contents like straight edges or big discontinuity changes of the surface. Accurate photogrammetric bundle adjustment, precise image registration and polygons refinement must be employed to reduce or minimize these geometric errors.

In the following, two methods of texture mapping of a Great Buddha niche are described. First, instead of the previously generated full mosaic, the original images are all oriented and mapped onto the 3D model (Section 5.1). In the second procedure we orient only the full mosaic and overlay it onto the 3D model of the niche (Section 5.2).

5.1   Multi-Image Texture

All the available images are imported in a photogrammetric bundle adjustment in order to recover the camera interior and exterior parameters. As input of the self-calibrating bundle adjustment, image coordinates of corresponding points, approximated object coordinates, approximations of camera positions and rotation angles as well as approximated camera

parameters are required. Figure 10 shows the recovered camera poses. Afterwards each oriented image is used for the texturing of the 3D model with our texture mapping software. The final textured model is exported into VRML-format for visualization.
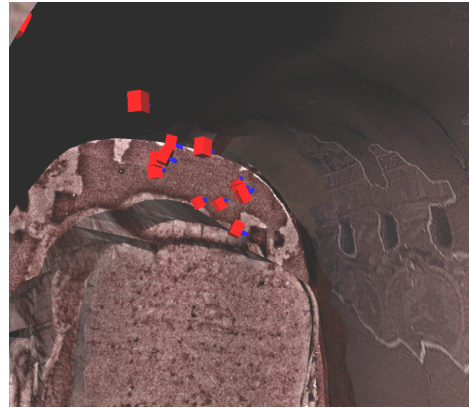

Figure 10: *The recovered camera poses. The images of the frescos were acquired from the head of the Great Buddha as well as from a cave on the western side of the niche (upper left corner).*

Because of the geometric as well as radiometric problems, the final multi-image texture mapping result was not satisfactory (Figure 11). The geometric inconsistencies are caused by small errors of the image orientation, as only a little a-priori knowledge was available. These errors of the photo-triangulation phase are then emphasised in the 3D textured model, in particular near the border between the different images. At these places also considerable radiometric differences appear. Although the original images can be equalized in the pre-processing stage, small inconsistencies remain. Because the final texture map consists of multiple images separately mapped onto the 3D surface, it is not easy to detect and remove them prior to the texture mapping phase.
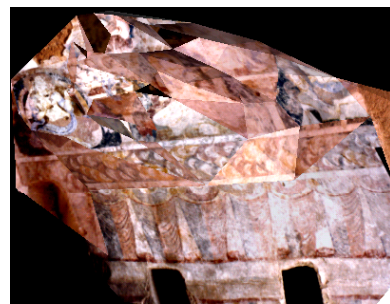

Figure 11: *The textured 3D model of the frescos. Different radiometric and geometric inconsistencies are visible in the rendered view.*

5.2   Full Mosaic Texture

After the generation of the full mosaic of the fresco using the constrained mesh-wise transformation, the two high-resolution images are oriented using a self-calibrating bundle-adjustment. Afterwards the oriented images are mapped onto the 3D geometric model and exported in
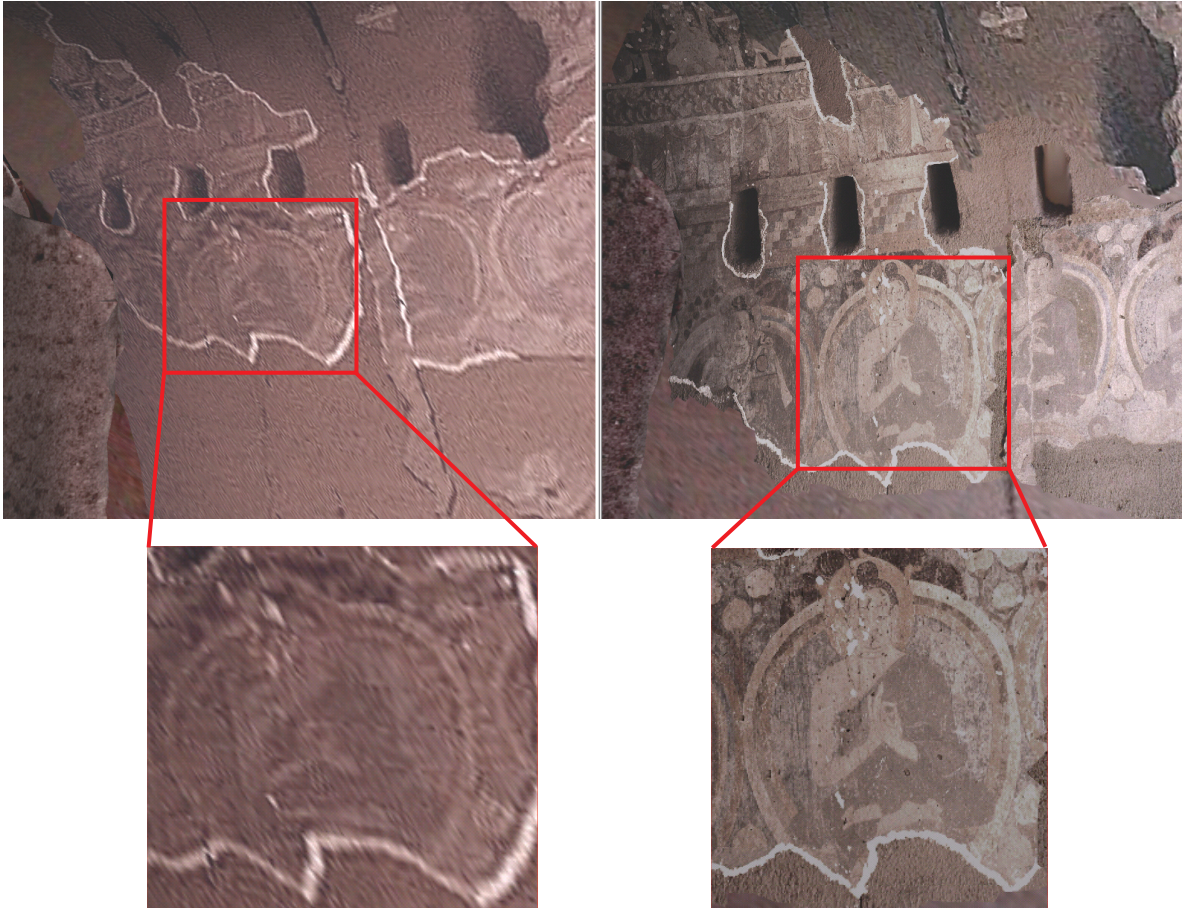
Figure 12: *A view of the 3D textured model of the frescos in the niche of the Great Buddha of Bamiyan, Afghanistan. On the left the textured 3D model obtained using the low-resolution images. On the right the textured 3D model created with the high-resolution frescos mosaic.*

VRML-format for visualization (Figure 12 and Figure 13). In this way the final photo-realistic model which fulfils the geometric and radiometric requirements of the movie makers is obtained.

Figure 13: *A closest view of the texture-mapped 3D model of the niche of the Great Buddha (upper mosaic).*

6. Conclusions

In this article we presented a novel method for the derivation of accurate high-resolution image mosaic using multi-resolution images acquired with different cameras and from arbitrary positions. The constrained mesh-wise affine transformation method showed the enhancement of the scene in the areas where higher resolution images are available and the preservation of edges straightness. The final photo-realistic 3D model fulfils now the required geometric and radiometric accuracy. On the other hand the other discussed approaches did not produce satisfactory and accurate results.

The presented image-based rendering and modeling shows the potential of these techniques, in particular in case of cultural heritage areas where only multi-resolution and multi-temporal images are available for the documentation and visualization of the scenes. The unique requirement is the existence of an 'overview' image to be used as master image in the transformation, which is a common case in this kind of applications.
Therefore the presented method for the derivation of high-resolution image mosaic can be easily used in many other fields like image restoration, text enhancements or computer generated special effects.

References

[Bal00] C. Baletti. Analytical and quantitative methods for the analysis of the geometrical content of historical cartography. *IAPRS*, Vol. XXXIII, Part B5, pp.30-37, 2000.

[BAM01] Bamiyan – Art and Archaeological Researches on the Buddhist cave Temples in Afghanistan 1970-1978. Publication of the Kyoto University Archaeological Mission to Central Asia. Edited by Prof. T.Higuchi, 4 Volumes, Dohosha Media Plan, 2001.

[BK00] S. Baker and T. Kanade, "Limits on Super-resolution and How to Break Them," *Proceedings of CVPR'2000*, pp. 372-279, 2000.

[BS98] S. Borman and R.L. Stevenson, "Spatial Resolution Enhancement of Low-Resolution Image Sequences: A Comprehensive Review with Directions for Future Research," *Technical Report,* University of Notre Dame, 1998.

[BR03] E. Beauchesne and S.Roy, "Automatic Relighting of Overlapping Textures of a 3D Model". Proceedings of CVPR, pp. 166-173, 2003.

[CB97] M. Chiang and T. Boult. Local blur estimation and superresolution. Proceedings of CVPR, pp 821-826, 1997.

[CZ98] D. Capel and Z. Zissermann. Automated mosaicing with super-resolution zoom. *Proceedings of CVPR98*, pp. 885-891, 1998.

[DTM96] P.E. Debevec, C.J. Taylor, and J. Malik. Modeling and rendering architecture from photographs: a hybrid geometry- and image-based approach. *SIGGRAPH 96 Conference Proceedings*, pages 11–20, 1996.

[EF97] M. Elad and A. Feuer. Restoration of Single Super-resolution Image from Several Blurred, Noisy and Down-sampled Measured Images. *IEEE Trans. on Image Processing*, Vol. 6, no. 12, pp. 1646-58, 1997.

[FSM98] T. Fuse, E. Shimizu, S. Morichi. A study on geometric correction of historical maps. *IAPRS*, Vol. XXXII, Part 5, pp. 543-548, 1998.

[GRZ04] A. Gruen, F. Remondino, L. Zhang. Photogrammetric Reconstruction of the Great Buddha of Bamiyan, Afghanistan. *The Photogrammetric Record*, Vol.19, No.107, pp. 177-199, 2004.

[HLM96] P. Havaldar, M.-S. Lee, and G. Medioni. View synthesis from unregistered 2-D images. *Proceedings of Graphics Interface '96*, pages 61–69, 1996.

[KP04] Kim S.J. and M. Pollefeys, "Radiometric Self-Alignment of Image Sequences". Proceedings of CVPR, pp. 645-651, 2004.

[IA00] M. Irani and P. Anandan. About direct methods. In Triggs, Zissermann, Szeliski edts, *Vision Algorithms: Theory and Practice*, LNCS, Springer Verlag, 2000.

[IP91] M. Irani and S. Peleg, "Improving Resolution by Image Restoration," *Computer Vision, Graphics, and Image Processing*, Vol. 53, pp. 231-239, 1991.

[MP94] S. Mann and R. Picard. Virtual Bellow: Constructing high quality stills from video. *International Conference on Image Processing*, pp. 363-367, 1994.

[Nie02] J. Niederöst. Landscape as a Historical Object: 3D-Reconstruction and Evaluation of a Relief Model from the 18th Century. *IAPRS*, Vol. XXXIV, Part 5/W3, 2002.

[NB95] W. Niem and H. Broszio. Mapping texture from multiple camera views onto 3D-object models for computer animation. *Proceedings of the International Workshop on Stereoscopic and Three Dimensional Imaging*, 1995.

[PA] Panoguide: www.panoguide.com

[PAD98] K. Pulli, H. Abi-Rached, T. Duchamp, L.G. Shapiro, W. Stuetzle. Acquisition and visualization of colored 3-D objects. Proc. *ICPR*, pp. 99-108, 1998.

[PAN] Panofactory: www.panoramafactory.com

[RCM02] C. Rocchini, P. Cignoni, C. Montani, R. Scopigno. Acquiring, stiching and blending diffuse appearance attributes on 3D models. *The Visual Computer*, 18, pp. 186-204, 2002.

[SZE94] R. Szeliski. Image mosaicing for tele-reality applications. TR, Digital Equipment Corporation, Cambridge, USA, 1994.

[UN] UNESCO World Heritage List: whc.unesco.org/

[VI] Video Investigator, Cognitech: www.cognitech.com

[VF] Video Focus, Salient Stills: www.salientstill.com

[VZG01] Visnovcova (Niederoest), J., Zhang, L., Gruen, A. Generating a 3D model of a Bayon tower using non-metric imagery. *IAPRS*, Vol. XXXIV, Part 5/W1, pp. 30-39, 2001.